Inorg. Chem. **2003**, *42*, 5173–5184

Electron Donor–Acceptor Dyads and Triads Based on Tris(bipyridine)ruthenium(II) and Benzoquinone: Synthesis, Characterization, and Photoinduced Electron Transfer Reactions

Magnus Borgström,[†] Olof Johansson,[‡] Reiner Lomoth,[†] Helena Berglund Baudin,[†] Staffan Wallin,[†] Licheng Sun,*[,‡] Björn Åkermark,*[,‡] and Leif Hammarström*[,†]

Department of Physical Chemistry, BMC, Uppsala University, PO Box 579, SE-751 23 Uppsala, Sweden, and Department of Organic Chemistry, Stockholm University, SE-106 91 Stockholm, Sweden

Received October 7, 2002

Two electron donor–acceptor triads based on a benzoquinone acceptor linked to a light absorbing $[Ru(bpy)_3]^{2+}$ complex have been synthesized. In triad **6** (denoted Ru^{II}–BQ–Co^{III}), a $[Co(bpy)_3]^{3+}$ complex, a potential secondary acceptor, was linked to the quinone. In the other triad, **8** (denoted PTZ–Ru^{II}–BQ), a phenothiazine donor was linked to the ruthenium moiety. The corresponding dyads Ru^{II}–BQ (**4**) and PTZ–Ru^{II} (**9**) were prepared for comparison. Upon light excitation in the visible band of the ruthenium moiety, electron transfer to the quinone occurred with a rate constant $k_f = 5 \times 10^9$ s^{-1} ($\tau_f = 200$ ps) in all the quinone containing complexes. Recombination to the ground state followed, with a rate constant $k_b \sim 4.5 \times 10^8$ s^{-1} ($\tau_b \sim 2.2$ ns), for both Ru^{II}–BQ and Ru^{II}–BQ–Co^{III} with no indication of a charge shift to generate the reduced Co^{II} moiety. In the PTZ–Ru^{II}–BQ triad, however, the initial charge separation was followed by a rapid ($k > 5 \times 10^9$ s^{-1}) electron transfer from the phenothiazine moiety to give the fairly long-lived PTZ$^{\bullet+}$–Ru^{II}–BQ$^{\bullet-}$ state ($\tau = 80$ ns) in unusually high yield for a $[Ru(bpy)_3]^{2+}$-based triad (> 90%), that lies at $\Delta G^\circ = 1.32$ eV relative to the ground state. Unfortunately, this triad turned out to be rather photolabile. Interestingly, coupling between the oxidized PTZ$^{\bullet+}$ and the BQ$^{\bullet-}$ moieties seemed to occur. This discouraged further extension to incorporate more redox active units. Finally, in the dyad PTZ–Ru^{II} a reversible, near isoergonic electron transfer was observed on excitation. Thus, a quasiequilibrium was established with an observed time constant of 7 ns, with ca. 82% of the population in the PTZ–*Ru^{II} state and 18% in the PTZ$^{\bullet+}$–Ru^{II}(bpy$^{\bullet-}$) state. These states decayed in parallel with an observed lifetime of 90 ns. The initial electron transfer to form the PTZ$^{\bullet+}$–Ru^{II}(bpy$^{\bullet-}$) state was thus faster than what would have been inferred from the *Ru^{II} emission decay ($\tau = 90$ ns). This result suggests that reports for related PTZ–Ru^{II} and PTZ–Ru^{II}–acceptor complexes in the literature might need to be reconsidered.

Introduction

Electron transfer reactions in molecular systems are fundamental components of life processes. One important example is photosynthesis, where sunlight is converted into chemical energy via creation of a light-induced charge-separated state.[1] Mimicking these photochemical reactions, to produce a stable chemical fuel in an artificial system, is a long-standing challenge.

A unique combination of photophysical and redox properties makes derivatives of tris(bipyridine)ruthenium(II) ($[Ru(bpy)_3]^{2+}$) ideal candidates for the role as photosensitizers for artificial photosynthetic systems.[2−4] We have shown previously how $[Ru(bpy)_3]^{2+}$ derivatives, upon oxidation by an external electron acceptor, can accept electrons from covalently linked tyrosine and manganese complexes.[5] In

* Corresponding author. E-mail: Leifh@fki.uu.se (L.H.).
[†] Uppsala University.
[‡] Stockholm University.

(1) Barber, J.; Andersson, B. *Nature* **1994**, *370*, 31−34.
(2) Juris, A.; Balzani, V.; Barigeletti, F.; Campagna, S.; Belser, P.; von Zelewsky, A. *Coord. Chem. Rev.* **1988**, *84*, 85−277.
(3) (a) Kalyanasundaram, K. *Photochemistry of Polypyridine and Porphyrin Complexes*; Academic Press: London, 1992. (b) Darwent, J. R.; Douglas, P.; Harriman, G. P.; Richoux, M.-C. *Coord. Chem. Rev.* **1982**, *44*, 83−126.
(4) Sauvage, J.-P.; Collin, J.-P.; Chambron, J.-C.; Guilleraz, S.; Coudret, C.; Balzani, V.; Barigelletti, F.; De Cola, L.; Flamigni, L. *Chem. Rev.* **1994**, *94*, 993−1019.

10.1021/ic020606j CCC: $25.00
Published on Web 07/19/2003

Scheme 1 [a]

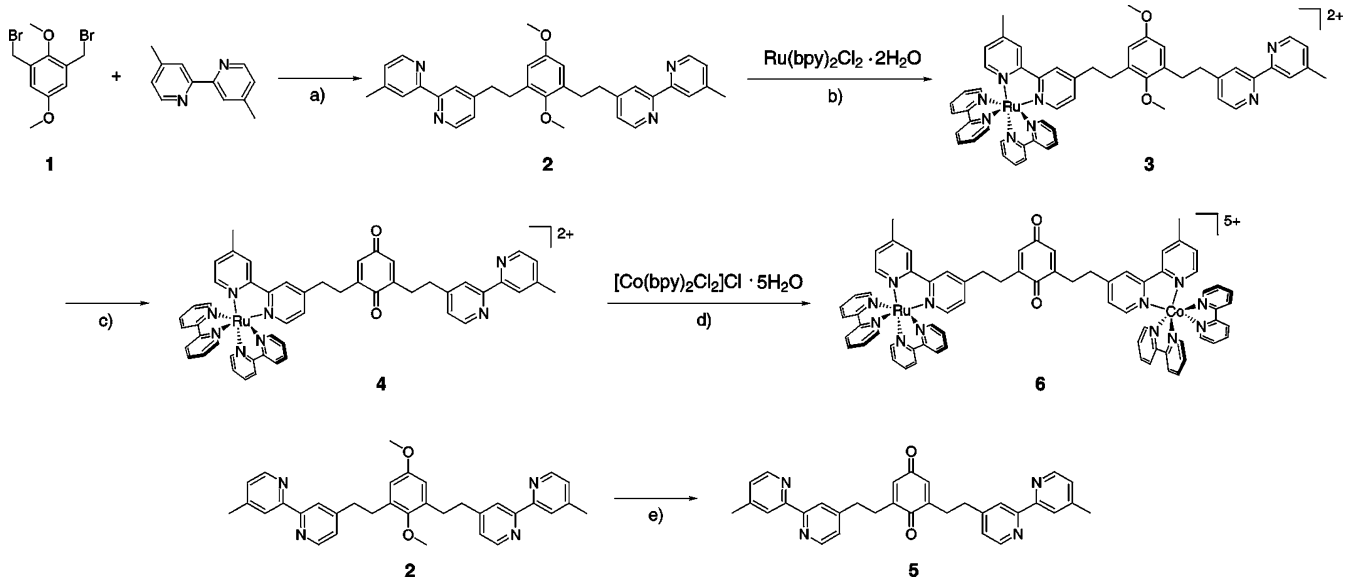

[a] Reaction conditions are as follows: (a) LDA, 2 equiv of 4,4′-dimethyl-2,2′-bipyridine, THF, −78 °C (78%); (b) 6 equiv of **2**, EtOH, reflux (67%); (c) 3 equiv of CAN, H_2O/CH_3CN, room temperature (72%); (d) MeOH, reflux (72%); (e) 3 equiv of CAN, 2 equiv of TsOH, room temperature (68%).

order to increase the reaction control, and also to increase the rate of the primary photooxidation of the $[Ru(bpy)_3]^{2+}$ unit, the use of acceptors that are covalently linked to the sensitizer is preferred. A common problem with these kinds of chromophore−acceptor dyads is a relatively rapid charge recombination reaction.[6−8] The recombination can often be slowed by incorporating an intermediate acceptor, forming a triad complex, thus increasing the distance between the charges. A long lifetime of the charge-separated state is important in order to allow further intermolecular chemical reactions to compete.

Several systems based on the more chlorophyll-like porphyrins have been successful in this respect.[6,7,9] It is difficult, however, to obtain an oxidation potential for a porphyrin as high as that for $[Ru(bpy)_3]^{2+}$, which is important for, e.g., water oxidation, and still maintain the necessary photophysical properties and the synthetic feasibility.[2−4]

For triads based on $[Ru(bpy)_3]^{2+}$, the reported formation yield of the charge-separated state has been moderate ($\leq$0.4),[10−15] presumably because recombination of the primary charge separation competed with further charge shift to form the fully charge-separated state. An exception is a PTZ−Ru^{II}−DQ complex (PTZ = phenothiazine, DQ = diquat) reinvestigated recently where the charge-separated state was formed with ca. 86% efficiency,[16] and not 25% as originally reported.[10]

In the present study, we use benzoquinone (BQ) as the primary acceptor. Quinones are of interest because of their relevance for natural photosynthesis, and they have been extensively used in electron transfer studies involving porphyrins and organic donors.[6,7] There are also a few examples where they are linked to $[Ru(bpy)_3]^{2+}$.[11,12,17,18] From a synthetic point of view, quinones are highly attractive, because they are noncharged species, and are easily functionalized, offering a wide range of redox potentials. For the secondary acceptor, we chose $[Co(bpy)_3]^{3+}$. This complex has a suitable redox potential for conversion into $[Co(bpy)_3]^{+}$, which is known to reduce substrates such as CO_2 or H^+.[19] A number of Ru^{II}−Co^{III} linked complexes have previously been shown to perform light-induced electron transfer to the Co^{III} unit.[20−22] We thus synthesized the Ru^{II}−BQ−Co^{III} triad **6** (Scheme 1). In this complex, we were unable to detect

(5) Sun, L.; Hammarström, L.; Åkermark, B.; Styring, S. *Chem. Soc. Rev.* **2001**, *30*, 36−49.
(6) Wasielewski, M. R. *Chem. Rev.* **1992**, *92*, 435−461.
(7) Gust, D.; Moore, T. A.; Moore, A. L. In *Electron Transfer in Chemistry*; Balzani, V., Ed.; Wiley-VCH: Weinheim, 2001, pp 272−336.
(8) Yonemoto, E. H.; Saupe, G. B.; Schmehl, R. H.; Hubig, S. M.; Riley, R. L.; Iverson, B. L.; Mallouk, T. E. *J. Am. Chem. Soc.* **1994**, *116*, 4786−4795.
(9) Imahori, H.; Guldi, D. M.; Tamaki, K.; Yoshida, Y.; Luo, C.; Sakata, Y.; Fukuzumi, S. *J. Am. Chem. Soc.* **2001**, *123*, 6617−6628.
(10) Danielson, E.; Elliott, C. M.; Merkert, J. W.; Meyer, T. J. *J. Am. Chem. Soc.* **1987**, *109*, 2519−2520.
(11) Opperman, K. A.; Mecklenburg, S. L.; Meyer, T. J. *Inorg. Chem.* **1994**, *33*, 5295−5301.
(12) Mecklenburg, S. L.; McCafferty, D. G.; Schoonover, J. R.; Peek, B. M.; Erickson, B. W.; Meyer, T. J. *Inorg. Chem.* **1994**, *33*, 2974−2983.
(13) (a) Larson, S. L.; Elliott, C. M.; Kelley, D. F. *J. Phys. Chem.* **1995**, *99*, 6530−6539. (b) Cooley, L. F.; Larson, S. L.; Elliott, C. M.; Kelley, D. F. *J. Phys. Chem.* **1991**, *95*, 10694−10700.
(14) Maxwell, K. A.; Sykora, M.; DeSimone, J. M.; Meyer, T. J. *Inorg. Chem.* **2000**, *39*, 71−75.
(15) Treadway, J. A.; Chen, P.; Rutherford, T. J.; Keene, F. R.; Meyer, T. J. *J. Phys. Chem. A* **1997**, *101*, 6824−6826.
(16) Klumpp, T.; Linsenmann, M.; Limoges, B. R.; Burssner, D.; Krissinel, E. B.; Elliott, C. M.; Steiner, U. E. *J. Am. Chem. Soc.* **1999**, *121*, 1076−1087.
(17) Berthon, R. A.; Colbran, S. B.; Moran, G. B. *Inorg. Chim. Acta* **1993**, *204*, 3−7.
(18) Goulle, V.; Harriman, A.; Lehn, J.-M. *J. Chem. Soc., Chem. Commun.* **1993**, 1034−1036.
(19) (a) Creutz, C.; Sutin, N. *Coord. Chem. Rev.* **1985**, *64*, 321−341. (b) Keene, F. R.; Creutz, C.; Sutin, N. *Coord. Chem. Rev.* **1985**, *64*, 247−260. (c) Szalda, D. J.; Creutz, C.; Mahajan, D.; Sutin, N. *Inorg. Chem.* **1983**, *22*, 2372−2379.
(20) Yoshimura, A.; Nozaki, K.; Ikeda, N.; Ohno, T. *J. Phys. Chem.* **1996**, *100*, 1630−1637.
(21) Komatsuzaki, N.; Himeda, Y.; Hirose, T.; Sugihara, H.; Kasuga, K. *Bull. Chem. Soc. Jpn.* **1999**, *72*, 725−731.

Scheme 2 [a]

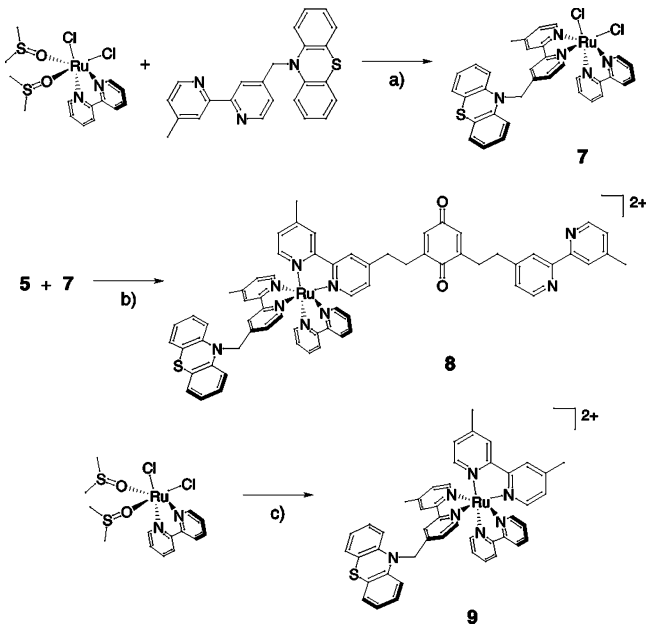

[a] Reaction conditions are as follows: (a) DMF, reflux; (b) ca. 6 equiv of **5**, EtOH, reflux (ca. 10%); (c) (1) 4,4′-dimethyl-2,2′-bipyridine, DMF, 120 °C; (2) PTZdmb, EtOH, reflux (21%).

any formation of reduced Co^{II} since the back electron transfer from reduced quinone to the Ru^{III} unit was too fast. To solve this problem, PTZ−Ru^{II}−BQ triad **8** (Scheme 2) was synthesized, to which the electron donor phenothiazine is attached. This substantially increased the charge separation lifetime. Stability problems, however, discouraged us from attempting the preparation of the tetrad PTZ−Ru^{II}−BQ−Co^{III}. Finally, in the model dyad PTZ−Ru^{II} (**9**) (Scheme 2) we observed a rapid formation (τ_{obs} = 7 ns) of the charge transfer state $PTZ^{\bullet+}$−$Ru^{II}(bpy^{\bullet-})$, in a quasiequilibrium with the PTZ−$^*Ru^{II}$ excited state. The near isoergonic charge separation was more rapid than what was indicated by the observed emission decay. This is important for a correct analysis of the reaction sequence in the PTZ−Ru^{II}−BQ triad **8**, viz. if the primary charge separation is oxidative quenching by the quinone, or reductive quenching by the phenothiazine.

Results

Synthesis. The synthetic routes for the preparation of the Ru^{II}−BQ dyad **4** and the Ru^{II}−BQ−Co^{III} triad **6** are described in Scheme 1. Compound **1**[23] was allowed to react with 2 equiv of deprotonated 4,4′-dimethyl-2,2′-bipyridine (dmb) in THF to give the symmetrical bis-bipyridine ligand **2**. Reaction of *cis*-$Ru(bpy)_2Cl_2 \cdot 2H_2O$ with an excess of **2** gave the mononuclear complex **3**, which was oxidized with Ce^{IV} to give Ru^{II}−BQ (**4**). Alternatively, quinone **5** was first prepared from **2** by reaction with Ce^{IV} in the presence of 2 equiv of strong acid and then with *cis*-$Ru(bpy)_2Cl_2 \cdot 2H_2O$ to give **4**. This dyad is a potential precursor to a multitude of binuclear complexes, bridged by a redox-active quinone. Reaction of **4** with 1 equiv of $[Co(bpy)_2Cl_2]Cl \cdot 5H_2O$ gave the dinuclear triad Ru^{II}−BQ−Co^{III} (**6**).

In order to increase the lifetime of the charge-separated state, we also synthesized PTZ−Ru^{II}−BQ triad **8**, which contains a linked phenothiazine donor (Scheme 2). The reaction between Ru(2,2′-bpy)$(DMSO)_2Cl_2$[24] and 10-((4′-methyl-2,2′-bipyridine-4-yl)methyl)phenothiazine (PTZdmb)[14,25] gave complex **7** and $Ru(PTZdmb)_2Cl_2$ in a ratio of ca. 3.5:1, indicating that some ligand scrambling had occurred during the reaction. The reaction of an excess of ligand **5** with **7** gave the mononuclear triad PTZ−Ru^{II}−BQ (**8**) in low yield. It should be stressed that care was taken to avoid light as much as possible during synthesis and purification. Because of the lability of triad **8**, we were not able to prepare the PTZ−Ru^{II}−BQ−Co^{III} tetrad.

The tris-heteroleptic PTZ−Ru^{II} complex **9** was also synthesized (Scheme 2) as a model for the PTZ−Ru^{II} unit in PTZ−Ru^{II}−BQ (**8**). This complex was chosen instead of the alternative bis-heteroleptic complexes $[Ru(dmb)_2(PTZdmb)]^{2+}$ or $[Ru(bpy)_2(PTZdmb)]^{2+}$ for which photophysical data were given by Meyer and co-workers,[11,15] in order to obtain more similar properties of the Ru^{II} moiety in the dyad and the triad. The stepwise addition of the three bipyridines starting from $Ru(DMSO)_4Cl_2$ gave the desired complex in low yield. All ruthenium complexes were isolated as PF_6^- salts.

The use of nonsymmetrical bidentate ligands necessarily leads to a mixture of different geometrical isomers.[26] The tris-heteroleptic complexes PTZ−Ru^{II}−BQ (**8**) and PTZ−Ru^{II} (**9**) can exist in four and two geometrical forms, respectively. The complexes were isolated as an approximately statistical mixture of isomers, as suggested by NMR (see Supporting Information).

Electrochemical Data. The redox properties of the dyad and triad complexes in dry acetonitrile were studied by cyclic voltammetry (CV) and differential pulse voltammetry (DPV). The electrochemical data are collected in Table 1. Half-wave potentials ($E_{1/2}$) were determined by cyclic voltammetry as the average of anodic and cathodic peak potentials ($E_{1/2} = (E_{pa} + E_{pc})/2$). Adsorption spikes were observed in the voltammograms of Ru^{II}−BQ (**4**), PTZ−Ru^{II}−BQ (**8**), and Ru^{II}−BQ−Co^{III} (**6**) after reduction to neutral or negative overall charge. Where CV waves were perturbed by these effects, half-wave potentials were determined from DPV peak potentials. The assignments given in Table 1 are based on comparison with data obtained for the model compounds $[Ru(bpy)_3]^{2+}$, $[Co(bpy)_3]^{3+}$, *p*-benzoquinone (BQ), and *N*-methylphenothiazine (MePTZ) obtained under the same conditions.

For Ru^{II}−BQ−Co^{III}, two reductions at $E_{1/2} = -0.105$ V and $E_{1/2} = -1.340$ V were observed that can be attributed to the metal-based reductions of the $[Co(bpy)_3]^{3+}$ moiety

(22) Song, X.; Lei, Y.; Van Wallendal, S.; Perkovic, M. W.; Jackman, D. C.; Endicott, J. F.; Rillema, D. P. *J. Phys. Chem.* **1993**, *97*, 3225−3236.
(23) Moran, V. J.; Schreiber, E. C.; Engel, E.; Behn, D. C.; Yamins, J. L. *J. Am. Chem. Soc.* **1952**, *74*, 127−129.
(24) Evans, I. P.; Spencer, A.; Wilkinson, G. *J. Chem. Soc., Dalton Trans.* **1973**, 204−209.
(25) Gould, S.; Strouse, G. F.; Meyer. T. J.; Sullivan, B. P. *Inorg. Chem.* **1991**, *30*, 2942−2949.
(26) Keene, F. R. *Coord. Chem. Rev.* **1997**, *166*, 121−159.

Table 1. Electrochemical Data for Complexes and Model Compounds

	$E_{1/2}{}^b$/V ($\Delta E_p{}^c$/mV)						
complex[a]	$[Ru(bpy)_3]^{2+/+}$	BQ^-/BQ^{2-}	$[Co(bpy)_3]^{2+/+}$	BQ/BQ^-	$[Co(bpy)_3]^{3+/2+}$	PTZ^+/PTZ	$[Ru(bpy)_3]^{3+/2+}$
$Ru^{II}-BQ$ (**4**)	−1.735 (131)	−1.560 (131)		−0.930 (89)			0.845 (89)
$Ru^{II}-BQ-Co^{III}$ (**6**)	−1.730 (−[d])	∼ −1.58[e] (−[d])	−1.340 (89)	−0.870 (−[d])	−0.105 (114)		0.837 (65)
$PTZ-Ru^{II}-BQ$ (**8**)	−1.785 (−[d])	−1.600 (−[d])		−0.930 (76)		0.390 (−[d])	0.810 (88)
$PTZ-Ru^{II}$ (**9**)	−1.770 (101)					0.400 (86)	0.815 (102)
$[Ru(bpy)_3]^{2+}$	−1.725 (69[f])						0.880 (75[f])
p-BQ		−1.630 (88)		−0.905 (80)			
MePTZ						0.315 (141)	
$[Co(bpy)_3]^{3+}$			−1.370 (79)		−0.080 (93)		

[a] Ionic complexes as PF_6^- salts. [b] In CH_3CN, 0.1 M $(n\text{-}C_4H_9)_4N(PF_6)$ vs Fc^+/Fc. [c] $\upsilon = 0.1$ V s^{-1}. [d] Irreversible CV wave or ill-defined reverse peak. Potential from DPV peak potential. [e] No CV peak. Very weak DPV peak. [f] $\upsilon = 0.05$ V s^{-1}.

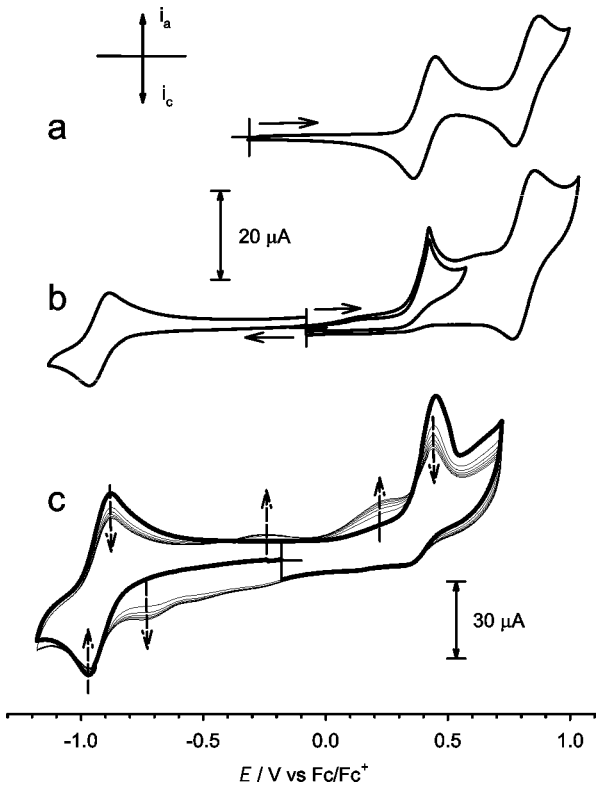

Figure 1. Cyclic voltammograms of $PTZ-Ru^{II}$ (1 mM, a) and $PTZ-Ru^{II}-BQ$ (1 mM, b,c) in acetonitrile with 0.1 M $N(n\text{-}C_4H_9)_4PF_6$ as supporting electrolyte. Scan rates: 0.1 V s^{-1} (a,b) and 1 V s^{-1} (c). Dashed arrows (c) indicate changes upon repeated cycling (scans 1−7).

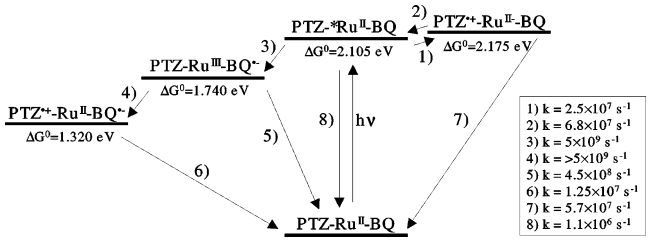

Figure 2. Summary of the reaction pathways and kinetics for the photoinduced electron transfers in $PTZ-Ru^{II}-BQ$. $\Delta G°$ for formation of the excited state was calculated from the 77 K emission maximum, which is close to the E_{00} value.[28]

($Co^{III} \rightarrow Co^{II} \rightarrow Co^{I}$). Under the same conditions, the Co^I state of the model complex $[Co(bpy)_3]^{3+}$ partly disproportionated already on the voltammetry time scale, and coulometrically, the reduction appeared to be a two-electron process on the time scale of bulk electrolysis ($Co^{II} \rightarrow Co^{I} \rightarrow Co^{0}$). For the triad $Ru^{II}-BQ-Co^{III}$, however, voltammetric peak heights indicated that both reductions of the $[Co(bpy)_3]^{3+}$ moiety are one-electron processes, i.e., that disproportionation of Co^I did not occur on the voltammetry time scale.

For the model compound MePTZ, the first oxidation ($PTZ \rightarrow PTZ^{\bullet+}$) is a reversible process, while further oxidation ($PTZ^{\bullet+} \rightarrow PTZ^{2+}$) is irreversible. For the triad $PTZ-Ru^{II}-BQ$, however, the first oxidation of the PTZ moiety appears to be irreversible under the same conditions (Figure 1b). The voltammogram of the dyad $PTZ-Ru^{II}$ (**9**) that lacks the BQ moiety shows a reversible wave attributable to the $PTZ^{\bullet+}/PTZ$ couple (Figure 1a), suggesting that the irreversibility of the PTZ oxidation in $PTZ-Ru^{II}-BQ$ arises from interaction of the PTZ cation radical with the BQ moiety. Further evidence for a reaction between $PTZ^{\bullet+}$ and the BQ moiety in $PTZ-Ru^{II}-BQ$ comes from the set of subsequent CVs shown in Figure 1c. The initial scan shows the unperturbed, reversible wave of the $BQ/BQ^{\bullet-}$ couple followed by the irreversible oxidation of PTZ. Subsequent scans over the same potential range show additional cathodic and anodic peaks that grow in at the expense of the BQ and PTZ peaks as indicated by the arrows in Figure 1c. When repeated scans were made over only the $BQ/BQ^{\bullet-}$ wave (from −0.20 to −1.20 V), the peak height did not decrease, and no additional peaks appeared, showing that $BQ^{\bullet-}$ is not reactive toward the neutral PTZ. Rather, it is $PTZ^{\bullet+}$ that seems to react with the BQ moiety in $PTZ-Ru^{II}-BQ$, thereby inducing the changes shown in Figure 1c.[27]

The electrochemical data were used to calculate the free energies for the different charge-separated states relative to the ground state (see Figure 2):

$$\Delta G° = E_{1/2}(\text{donor}^{n+1/n}) - E_{1/2}(\text{acceptor}^{n/n-1}) \qquad (1)$$

(neglecting the relatively small work term). The excited state energy was calculated from the low-temperature emission data (see later).

Absorption Spectra. The UV−vis absorption maxima for the complexes are given in Table 2. The spectra of $Ru^{II}-BQ$ (**4**), $Ru^{II}-BQ-Co^{III}$ (**6**), and $PTZ-Ru^{II}-BQ$ (**8**) are shown in Figure 3. The spectra in the visible region are dominated by $d \rightarrow \pi^*$ MLCT bands of the ruthenium moiety

(27) The stability of electrochemically prepared $MePTZ^{\bullet+}$ was not affected by the presence of BQ, and no reaction products could be detected voltametrically.

Table 2. Absorption and Luminescence Data of Complexes in CH_3CN

complex[a]	absorption λ_{max} [nm] ($\epsilon \times 10^4$ [M^{-1} cm^{-1}])	emission λ_{max}[d] [nm] ($\phi_{em,rel}$)[e]
Ru^{II}−BQ (**4**)	454 (1.2), 288 (8.1), 250 (4.1)	584 (<0.01)
Ru^{II}−BQ−Co^{III} (**6**)	454 (1.2), 314 (sh, 3.2), 288 (8.5), 240 (sh, 7.1), 210 (sh, 10.2)	584 (<0.01)
PTZ−Ru^{II}−BQ (**8**)[b]	459 (1.5), 286 (8.5), 251 (7.6)	589 (<0.01)
PTZ−Ru^{II} (**9**)	458 (1.5), 288 (8.5), 253 (5.8)	589 (0.10)
$[Ru(bpy)_3]^{2+}$ [c]	451 (1.4), 288 (7.9), 254 (sh, 2.1), 244 (2.4)	582 (1.0)
$[Co(bpy)_3]^{3+}$	318 (sh, 2.6), 308 (3.0), 222 (7.8)	

[a] PF_6^- as counterions. [b] Normalized at MLCT band of **9**. [c] Anderson et al.[29] [d] Recorded at 77 K. The value is close to the value obtained from a spectral fit as shown before for similar complexes.[30] [e] Relative emissions as compared to $[Ru(bpy)_3]^{2+}$. $\phi_{ems} = 0.059$ for $[Ru(bpy)_3]^{2+}$.[2]

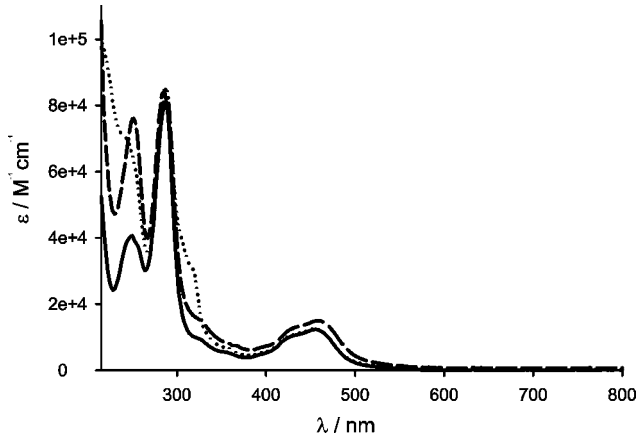

Figure 3. UV−vis absorption spectra of Ru^{II}−BQ (—), PTZ−Ru^{II}−BQ (- - -), and Ru^{II}−BQ−Co^{III} (····) in CH_3CN.

and in the UV region by ligand-centered $\pi \rightarrow \pi^*$ transitions.[2] This allowed selective excitation of the complexes in the 400−500 nm region. The additional 4,4′-dimethyl-2,2′-bpy ligand in PTZ−Ru^{II} (**9**) and PTZ−Ru^{II}−BQ red-shifted the MLCT band by a few nanometers and increased the extinction coefficient somewhat (Table 2). The presence of PTZ, Co^{III}, or BQ moieties gave rise to additional UV bands. All electronic absorption spectra can be described as the sum of the component spectra, indicating that the intercomponent interaction is weak.

Emission Measurements. The emission spectra for the triads and dyads both in butyronitrile at 77 K and in acetonitrile at room temperature, were typical for the ^{3}MLCT excited state of $[Ru(bpy)_3]^{2+}$-type complexes (Table 2).[2,28] The intensity of the room-temperature emission was greatly reduced in the dyads and the triads compared to $[Ru(bpy)_3]^{2+}$, indicating a fast quenching of the ruthenium-based ^{3}MLCT excited state by both the appended phenothiazine and benzoquinone units. In PTZ−Ru^{II} (**9**), the emission intensity was reduced to 10% of that for $[Ru(bpy)_3]^{2+}$. Time-resolved measurements showed a single exponential emission decay with a lifetime of 90 ns, which is only 10% of that for $[Ru(bpy)_3]^{2+}$. In Ru^{II}−BQ (**4**), the emission intensity was reduced to <1% of that for $[Ru(bpy)_3]^{2+}$. No time-resolved emission could be seen on the time scale of nanosecond flash photolysis, suggesting a lifetime < 10 ns. This is in agreement with the transient absorption data described in a following paragraph. The data for Ru^{II}−BQ−Co^{III} (**6**) were essentially identical to those for Ru^{II}−BQ.

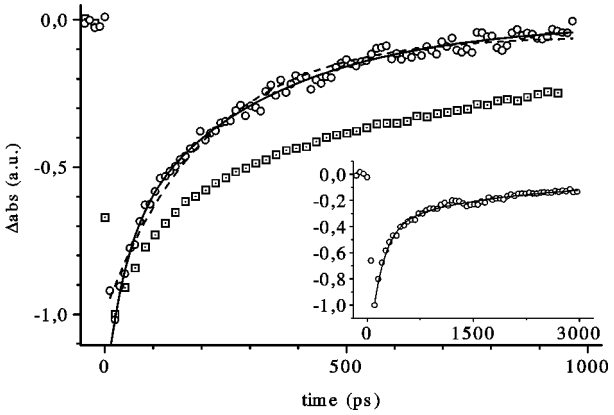

Figure 4. Transient absorption kinetic traces of Ru^{II}−BQ (⊡) and PTZ−Ru^{II}−BQ (○) probed at 450 nm. The dashed (- - -) and solid (—) lines in the main figure are double and single exponential fits to the data. The inset shows transient absorption changes at 450 nm for Ru^{II}−BQ followed on a longer time scale. The line is a double exponential fit to the data.

For PTZ−Ru^{II}−BQ (**8**), the emission intensity was as small as that for Ru^{II}−BQ. For PTZ−Ru^{II}−BQ, however, a weak ruthenium-based emission was detected in the time-resolved measurements, with a lifetime of 65 ns. This emission component increased in magnitude when the complex was exposed to an increasing number of laser flashes.

In both of the PTZ-containing complexes PTZ−Ru^{II}−BQ and PTZ−Ru^{II}, a new short-lived (<10 ns) emission, centered around 530 nm, grew in with increasing number of flashes given to the sample. Because the complexes were sensitive to light, all measurements were performed in the dark, and the data presented is for freshly prepared samples exposed to a minimum number of excitation flashes.

Transient Absorption Measurements. The light-induced reactions in the dyads and the triads were investigated by transient absorption changes following excitation with 150 fs pulses at either 400 or 480 nm. For time scales above 5 ns, a flash photolysis setup was used with <10 ns excitation flashes at 460 nm.

Ru^{II}−BQ (4). The excited state of Ru^{II}−BQ decayed with a lifetime of ca. 200 ps, as shown by the decay of the transient absorption at 370 nm (not shown) and the recovery of the bleach at 450 nm (Figure 4). At 450 nm, the transient signal from the ruthenium moiety resulted in a similar bleach for both the excited and the oxidized states. However, the quinone radical absorption around 450 nm compensated for that in the Ru^{III}−$BQ^{\bullet-}$ state, resulting in very small net bleach. A double exponential fit to the trace at 450 nm gave $\tau = 200$ ps for the first exponent and $\tau \sim 2.2$ ns for the second. A fit to the data at 370 nm gave a similar result. The first exponent is attributed to electron transfer from excited ruthenium to the benzoquinone, and the second exponent is attributed to the recombination reaction to the ground state.

Ru^{II}−BQ−Co^{III} (6). The transient absorption results for Ru^{II}−BQ−Co^{III} (not shown) were identical to those for Ru^{II}−

(28) Hager, C. D.; Crosby, G. A. *J. Am. Chem. Soc.* **1975**, *97*, 7031−7037.

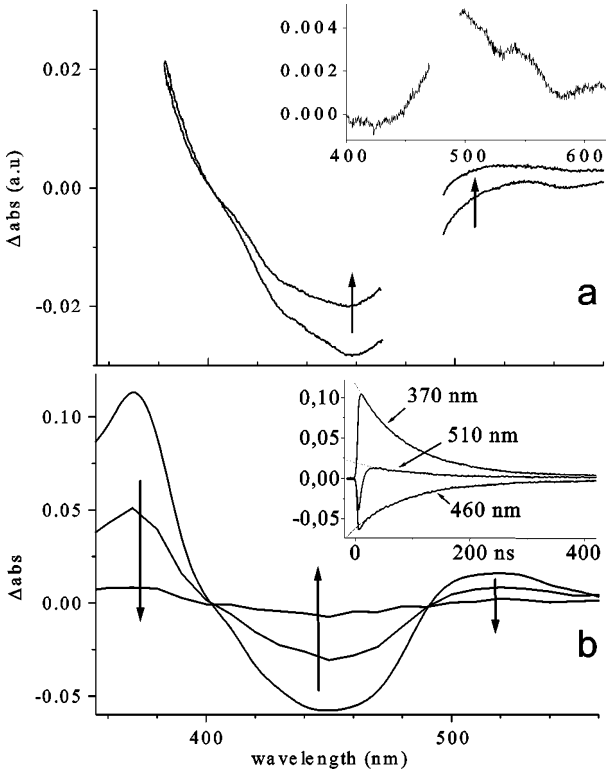

Figure 5. Transient absorption spectrum of PTZ−Ru^{II} following excitation with a 150 fs (a) or ca. 5 ns (b) laser pulse. (a) $t = 4$ ps and 4 ns. The inset shows the absorption spectrum of the charge transfer state $PTZ^{\bullet+}-Ru^{II}(bpy^{\bullet-})$ after 4 ns (see text). (b) $t = 40$, 120, and 360 ns. Inset shows kinetic traces at 370, 460, and 510 nm.

BQ, within experimental error, and we were not able to detect any long-lived transient from the $Ru^{III}-BQ-Co^{II}$ state, neither on the picosecond time scale in the pump−probe experiments nor with nanosecond flash photolysis.

PTZ−Ru^{II} (9). In Figure 5b, the transient absorption spectrum for PTZ−Ru^{II} is shown at 40, 120, and 360 ns after a laser flash. The spectrum is very similar to that of the $*Ru^{II}$ excited state, which displays a ground state bleaching around 452 nm ($\Delta\epsilon_{452} = -1.0 \times 10^4$ M^{-1} cm^{-1})[2] and an absorption from the reduced $bpy^{\bullet-}$ ligand in the ^{3}MLCT state (formally $Ru^{III}(bpy^{\bullet-})(bpy)_2$) with a maximum at 370 nm ($\Delta\epsilon_{370} = 2.0 \times 10^4$ M^{-1} cm^{-1}).[31] However, the absorption around 510 nm is significantly larger than expected for the excited state alone ($\Delta\epsilon_{510} < 500$ M^{-1} cm^{-1}).[31] Instead, it seems that the spectra reflect a mixture of the excited and charge transfer states, since both the reduced $Ru^{II}(bpy^{\bullet-})(bpy)_2$ ($\Delta\epsilon_{510} = 1.0 \times 10^4$ M^{-1} cm^{-1})[32] and oxidized $PTZ^{\bullet+}$ ($\Delta\epsilon_{510} = 5.0 \times 10^3$ M^{-1} cm^{-1})[33] give significant absorption at this wavelength. In Figure 5a, the evolution of the transient absorption spectrum is shown on a shorter time scale. At 4 ps after excitation with a 150 fs laser pulse, the spectrum is consistent with the excited state, while the spectrum at 4 ns shows an increased absorption above 480 nm. The inset shows the difference spectrum when the excited state features have been subtracted from the spectrum at 4 ns. The difference spectrum can be attributed to the $PTZ^{\bullet+}-Ru^{II}(bpy^{\bullet-})$ charge transfer state, with significant contribution from both the reduced ruthenium and the oxidized PTZ moieties. The kinetic trace in the inset of Figure 6 shows the build up of the absorption at 510 nm, that is followed to the end of the optical delay line of the pump−probe setup. The rise could not be followed to completion with this method, but no rise in the 510 nm absorption could be observed with nanosecond flash photolysis (ca. 10−15 ns detection limit). A single exponential fit to the trace in the inset of Figure 6 gave a lifetime of 7 ns for the absorption rise, which is consistent also with the nanosecond data. This shows that a partial charge separation in the excited PTZ−Ru^{II} is established with a time constant of ca. 7 ns. From the differential extinction coefficients at 370 and 510 nm for the different states, we could calculate that the fraction of charge transfer state after 40 ns (Figure 5b) was 18%. The transient absorption shown in Figure 5b, as well as the emission, showed a single exponential decay with $\tau = 90$ ns at all wavelengths 300−600 nm. This suggests that a quasiequilibrium was established between the excited and charge transfer states, and that these states decayed to the ground state with a common 90 ns overall time constant (see Discussion section).

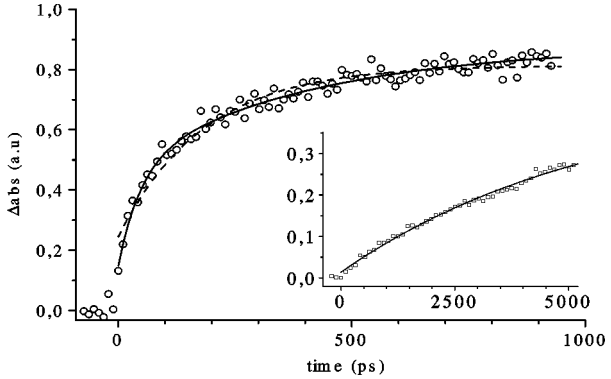

Figure 6. Transient absorption traces probed at 510 nm for PTZ−Ru^{II}−BQ (○) and PTZ−Ru^{II} (inset, □), following excitation with a 150 fs pulse. The dashed (- - -) and solid (—) lines in the main figure are double and single exponential fits to the data.

When the experiments were performed in the more polar solvent formamide, the fraction of charge transfer in the quasiequilibrium was 27% instead of 18%. This may be expected, as charge-separated states are in general stabilized in polar media. The transient absorption and emission decay were still single exponential, but somewhat faster ($\tau = 60$ ns) than in acetonitrile.

(29) Anderson, P. A.; Deacon, G. B.; Haarmann, K. H.; Keene, F. R.; Meyer, T. J.; Reitsma, D. A.; Skelton, B. W.; Strouse, G. F.; Thomas, N. C.; Treadway, J. A.; White, A. H. *Inorg. Chem.* **1995**, *34*, 6145−6157.

(30) (a) Caspar, J. V.; Meyer, T. J. *Inorg. Chem.* **1983**, *22*, 2444−2453. (b) Hammarström, L.; Barigelletti, F.; Flamigni, L.; Indelli, M. T.; Armaroli, N.; Calogero, G.; Guardigli, M.; Sour, A.; Collin, J.-P.; Sauvage, J.-P. *J. Phys. Chem. A* **1997**, *101*, 9061−9069. (c) Treadway, J. A.; Loeb, B.; Lopez, R.; Anderson, P. A.; Keene, F. R.; Meyer, T. J. *Inorg. Chem.* **1996**, *35*, 2242−2246.

(31) Yoshimura, A.; Hoffman, M.; Sun, H. *J. Photochem. Photobiol., A* **1993**, *70*, 29−33.

(32) (a) Mulazzani, Q. G.; Emmi, S.; Fuochi, P. G.; Hoffman, M. Z.; Venturi, M. *J. Am. Chem. Soc.* **1978**, *100*, 981−983. (b) Anderson, C. P.; Salmon, D. J.; Meyer, T. J.; Young, R. C. *J. Am. Chem. Soc.* **1977**, *99*, 1980−1982.

(33) (a) Alkaitis, S. A.; Beck, G.; Grätzel, M. *J. Am. Chem. Soc.* **1975**, *97*, 523−29. (b) Shine, H. J.; March, E. E. *J. Org. Chem.* **1965**, *30*, 2130−2139.

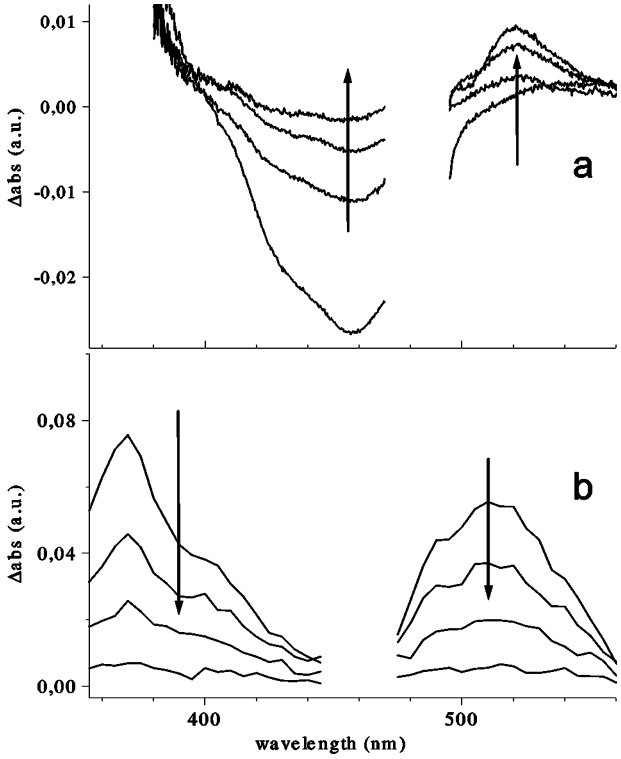

Figure 7. Transient absorption spectra of PTZ−Ru^{II}−BQ following excitation with a 150 fs (a) or ca. 5 ns (b) laser pulse. (a) $t = 4$, 100, 400, and 1000 ps. (b) $t = 22$, 50, 150, and 250 ns.

PTZ−Ru^{II}−BQ (8). Figure 7a shows the transient absorption spectrum for PTZ−Ru^{II}−BQ on the picosecond time scale. The initial ruthenium excited state features, with a strong ground state bleach around 450 nm, quickly disappear. Concomitantly, a build up of absorption around 510 nm is seen that can be attributed to the $PTZ^{\bullet+}$ radical, presumably in the fully charge-separated state $PTZ^{\bullet+}-Ru^{II}-BQ^{\bullet-}$. In Figure 7b, the transient spectra on the nanosecond time scale are shown. Also, a strong absorption from $PTZ^{\bullet+}$ around 510 nm is seen here, as well as a prominent absorption at 370 ns from the PTZ−*Ru^{II}−BQ excited state (see Discussion section). The expected positive differential absorption around 450 nm from the reduced $BQ^{\bullet-}$ ($\Delta\epsilon_{450} = 7000\ M^{-1}\ cm^{-1}$)[34] is not seen in either of the spectra. The results suggest that there is a bleaching around 450 nm from a long-lived fraction of the *Ru^{II} excited state that masks the $BQ^{\bullet-}$ absorption from the charge-separated state in the intact triads (see Discussion section).

The kinetic traces for PTZ−Ru^{II}−BQ at 450 and 510 nm are displayed in Figures 4 and 6. The build up of absorption at 510 nm follows very similar kinetics as the bleach recovery at 450 nm. A single exponential fit to the trace at 450 nm gave a lifetime, $\tau = 210$ ps. With a double exponential fit ($\tau_1 \sim 50$ ps (40%), $\tau_2 \sim 300$ ps (60%)), a better residual was obtained, but the average lifetime was similar, $\tau_{average} = 200$ ps. At 510 nm, the kinetic trace was fitted with $\tau = 180$ ps (1 exp) and $\tau_{average} = 180$ ps (2 exp). A similar value was obtained for the decay of the 370 nm absorption (not shown), which monitors the decay of the *Ru^{II} excited state. Thus, the oxidized $PTZ^{\bullet+}$ radical is formed with the same kinetics (within the experimental error) as that for both the *Ru^{II} excited state decay and for the Ru^{II} ground state recovery. The transient absorption spectrum thus produced decays on a much slower (ns) time scale, due to recombination to the ground state (Figure 7b). The decay kinetics was the same at all wavelengths and could be fitted with a single exponential function with a lifetime of 80 ns.

Experiments were performed to rule out possible effects of two-photon excitations (e.g., the $BQ^{\bullet-}$ species, which is formed within the duration of the excitation pulse in the nanosecond experiments, absorbs at the excitation wavelength). The excitation light was varied about an order of magnitude, and the signal magnitudes were compared for the triad and an isoabsorptive sample of $[Ru(bpy)_3]^{2+}$. The variation in the transient absorption amplitude was the same for both samples, showing that successive absorption of more than one photon by one triad molecule was not significant.

As in the described emission experiments, the transient absorption experiments indicate that PTZ−Ru^{II}−BQ is very photolabile. The absorption intensity at 370 nm after 20 ns (that is mainly from the excited state, see Discussion) grows with an increased number of laser flashes, in parallel to the increase in peak emission intensity. This effect is not seen at 510 nm.

Discussion

Our complexes were designed to perform efficient electron transfer from the optically induced excited state of the $[Ru(bpy)_3]^{2+}$ chromophore. The Ru^{II}−BQ (**4**) and PTZ−Ru^{II} (**9**) dyads serve as references for the interpretation of the results for the PTZ−Ru^{II}−BQ (**8**) and Ru^{II}−BQ−Co^{III} (**6**) triads.

Ru^{II}−BQ. In Ru^{II}−BQ, the forward electron transfer reaction from the excited ruthenium moiety

$$Ru^{II}-BQ \xrightarrow{k_f} Ru^{III}-BQ^{\bullet-} \xrightarrow{k_b} Ru^{II}-BQ \qquad (2)$$

occurred with a time constant of ca. 200 ps ($k_f = 5 \times 10^9\ s^{-1}$). The subsequent back reaction to regenerate the ground state was slower ($k_b \sim 4.5 \times 10^8\ s^{-1}$). This is in fair agreement with a previous report.[18]

Ru^{II}−BQ−Co^{III}. Although the charge shift reaction (eq 3) from the doublet $^2BQ^{\bullet-}$ to the ground state quartet (^4T) Co^{II} is spin forbidden, generation of the excited doublet (^2E) Co^{II} is spin allowed.

$$Ru^{III}-BQ^{\bullet-}-Co^{III} \xrightarrow{k_{sh}} Ru^{III}-BQ-Co^{II} \qquad (3)$$

The ^2E state is ca. 0.18 eV above the ground state ^4T,[19] which would give $\Delta G^\circ = -0.58$ eV for electron transfer to generate the ^2E state. Thus, the reduction of the Co^{III} complex via the ^2E state, followed by spin relaxation to the ^4T ground state, could be rapid, as has been observed for direct electron transfer from *Ru^{II} to Co^{III} in covalently linked complexes.[20−22] Since the transient signals from Ru^{II}−BQ−Co^{III} and Ru^{II}−BQ were identical, apparently the charge shift reaction was not able to compete with the recombination reaction ($k_b \sim$

(34) Darwent, J. R.; Kalyanasundaram, K. *J. Chem. Soc., Faraday Trans. 2* **1981**, *77*, 373−382.

Scheme 3

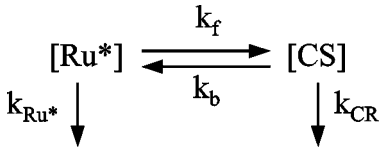

4.5×10^8 s^{-1}, eq 2). We thus estimate an upper limit for the charge shift rate constant in eq 3 to $k_{sh} < 5 \times 10^7$ s^{-1}.

PTZ−Ru^{II}. The PTZ−Ru^{II} dyad was synthesized and investigated in detail as a model system to understand the reactions in the PTZ−Ru^{II}−BQ triad. Therefore, the Ru^{II} moiety of PTZ−Ru^{II} is tris-heteroleptic with two 4,4′-bis-alkyl substituted bipyridine ligands and one unsubstituted ligand, in order to closely match the properties of the PTZ−Ru^{II} unit in the triad. Both the emission and the transient absorption spectra in the dyad decayed with a 90 ns lifetime, and the spectra showed features mainly of the excited state. Thus, one may at first believe that the 90 ns time constant reflects the initial charge separation, generating the PTZ$^{\bullet+}$ and the reduced Ru^{II}(bpy$^{\bullet-}$) moieties. The recombination reaction to the ground state would then have to be much faster, so that the charge transfer state PTZ$^{\bullet+}$−Ru^{II}(bpy$^{\bullet-}$) is never detected. In contrast, our data show that the initial electron transfer is much faster than the 90 ns suggests, and that a quasiequilibrium is established between the excited and the charge transfer states (Scheme 3).

That this is the case is quite clear from the absorption rise at 510 nm with $\tau = 7$ ns (Figure 6), where the charge transfer state absorbs, and the fact that the resulting transient spectrum deviates from that for the pure excited state (compare the spectra after 4 ps and 4 ns in Figure 5a). Once the quasiequilibrium is established, 82% of the population is in the excited state PTZ−*Ru^{II} and 18% is in the charge transfer state PTZ$^{\bullet+}$−Ru^{II}(bpy$^{\bullet-}$). Assuming a Boltzmann distribution, these values suggest a reaction free energy $\Delta G° = 0.044$ eV for the initial electron transfer. This is in good agreement with the electrochemical results that suggest $\Delta G° = 0.070$ eV. The quasiequilibrium is maintained throughout the decay to the ground state, as shown by the fact that the transient absorption spectrum keeps the same shape and decays with the same kinetics at all wavelengths on the >20 ns time scale. The observed 90 ns decay reflects the simultaneous decay of the excited and charge transfer states via the two different routes available: charge recombination (k_{CR}) and intrinsic excited state deactivation (k_{Ru*}). From our data, we could calculate the individual rate constants in Scheme 3 (see Supporting Information). Thus, we obtained $k_f = 2.5 \times 10^7$ s^{-1} and $k_b = 6.8 \times 10^7$ s^{-1} for the initial charge transfer and the reverse reaction. For the recombination reaction and the intrinsic excited state decay, we obtained $k_{CR} = 5.7 \times 10^7$ s^{-1} and $k_{Ru*} = 1.1 \times 10^6$ s^{-1}, respectively.

Although the quasiequilibrium was at all times shifted to the intrinsically more long-lived excited state, most of the excited state decay occurred via recombination of the more short-lived charge transfer state. The steady state emission quenching results gave a 10% emission yield for the PTZ−Ru^{II} dyad relative to [Ru(bpy)$_3$]$^{2+}$, suggesting that 90% of the decay occurs via the charge-separated state. This correlates well with calculations based on the kinetic data: the amount of the quasiequilibrium population decaying via k_{Ru*} and k_{CR} is proportional to k_{Ru*}[Ru*] and k_{CR}[CS], respectively. Thus, about 8% of the excited state decay proceeded via the intrinsic pathway and 92% via the charge transfer state PTZ$^{\bullet+}$−Ru^{II}(bpy$^{\bullet-}$), in good agreement with the steady state emission quenching results.

Due to the quasiequilibrium, the time constant for reductive quenching of PTZ−Ru^{II} is much smaller than the $\tau =$ 90 ns value one would obtain directly from the decay of the excited state emission or absorption features. Thus, the time constant for the reductive quenching step is actually 40 ns. However, the excited state decay is only dependent on the relative magnitude of the rate constants k_f and k_b (Scheme 3), and on the decay constants k_{CR} and k_{Ru*}, but it is not dependent on the absolute values of k_f and k_b. Thus, the error in estimating k_f if the quasiequilibrium is ignored can in general be much larger than in the present case. It is interesting therefore to compare our data with data for the similar PTZ−Ru^{II} complexes previously presented in the literature. For example, in [Ru(dmb)$_2$(PTZdmb)]$^{2+}$ [15] and [Ru^{II}(bpy)$_2$(PTZdmb)]$^{2+}$,[11] the driving force for reductive quenching is small ($\Delta G° \sim +0.1$ and -0.1 eV, respectively).[35] The rate constants for reductive quenching were calculated directly from the excited state decay kinetics. For [Ru(dmb)$_2$(PTZdmb)]$^{2+}$, the rate was estimated to ca. 4×10^5 s^{-1} from luminescence quenching data, and for [Ru^{II}(bpy)$_2$(PTZdmb)]$^{2+}$, the rate was reported to be $\geq 2.8 \times 10^8$ s^{-1}. The driving force in the present PTZ−Ru^{II} is intermediate between these two cases. It is quite possible that the excited state decay follows a quasiequilibrium between the excited and charge transfer states in all these complexes in which the driving force is close to zero. In that case, a change in $\Delta G°$ from $+0.1$ to -0.1 eV would change the relative population in the quasiequilibrium from about 1% to about 99% charge transfer. Given the approximate values of $\Delta G°$, this would be in agreement with the reported rate differences. In a different study, Elliott and co-workers reported electron transfer rates in a series of PTZ−Ru^{II} dyads with a range of driving forces and used a Marcus-type free-energy relationship analysis.[36] The rate constants were derived directly from the observed excited state decay kinetics, and the possibility of a quasiequilibrium was not considered. Particularly for the endoergonic and weakly exoergonic reactions, the discrepancy between the rate constants for the observed emission decay and the actual charge separation step could be significant.

PTZ−Ru^{II}−BQ. The ground state bleach at 450 nm (Figure 7a) is characteristic for the excited, oxidized, and reduced ruthenium moiety. Thus, the bleach recovery can be attributed to repopulation of the Ru^{II} ground state of PTZ−Ru^{II}−BQ, in combination with an increased absorption due

(35) No $\Delta G°$ value was given in ref 11. The value we report is our estimate based on data for substituent effects on [Ru(bpy)$_3$]$^{2+}$ excited state energies and redox potentials, see ref 2.

(36) Larson, S. L.; Elliott, S. M.; Kelley, D. F. *Inorg. Chem.* **1996**, *35*, 2070−2076.

to formation of the reduced $BQ^{\bullet-}$. The increase in absorption at 510 nm in the same figure is due to the formation of the $PTZ^{\bullet+}$. The 450 nm recovery and the 510 nm increase follow the same kinetics (compare traces in Figures 4 and 6) with a lifetime of ca. 200 ps. The decay of the 370 nm absorption from the $*Ru^{II}$ excited state follows similar kinetics. Consequently, the formation of the fully charge-separated state from the excited state occurs with a lifetime of 200 ps ($k_f = 5 \times 10^9\ s^{-1}$). There are two plausible pathways for this reaction: either via initial oxidative quenching of the $*Ru^{II}$ state by the BQ moiety (eq 4), or via initial reductive quenching by PTZ (eq 5).

$$PTZ-*Ru^{II}-BQ \rightarrow PTZ-Ru^{III}-BQ^{\bullet-} \rightarrow PTZ^{\bullet+}-Ru^{II}-BQ^{\bullet-} \quad (4)$$

$$PTZ-*Ru^{II}-BQ \rightarrow PTZ^{\bullet+}-Ru^{II}(bpy^{\bullet-})-BQ \rightarrow PTZ^{\bullet+}-Ru^{II}-BQ^{\bullet-} \quad (5)$$

None of the intermediate states could be detected, showing that the observed lifetime is that for the rate determining first reaction step, while the subsequent charge shift must be much more rapid. The results for the model dyad PTZ−Ru^{II} show that the reductive quenching is too slow ($k_f = 2.5 \times 10^7\ s^{-1}$) to explain the kinetics of the triad. Instead, the oxidative quenching kinetics in Ru^{II}−BQ is in excellent agreement with the triad kinetics ($k_f = 5 \times 10^9\ s^{-1}$). We therefore conclude that the charge separation in PTZ−Ru^{II}−BQ occurs via initial oxidative quenching by the quinone (eq 4), and that the subsequent charge shift, moving the oxidative equivalent from Ru^{III} to PTZ, occurs with a rate constant $>5 \times 10^9\ s^{-1}$. The noticeable deviation from single exponential kinetics (Figures 4 and 6) could possibly be ascribed to the expected presence of four different isomers of the triad, that may have somewhat different properties (e.g., cis-/trans-effects of substituents). Meyer and co-workers have reported some differences in the recombination kinetics between isomers of related triads.[15] We noted no deviation from single exponential kinetics in the recombination reaction, however. The decay of the transient spectrum represents the recombination of the charge-separated state, with a lifetime of 80 ns ($k = 1.25 \times 10^7\ s^{-1}$). A reaction scheme for PTZ−Ru^{II}−BQ is presented in Figure 2 where all the electron transfer rate constants are summarized. The recombination rate constants for the intermediates are assumed to be the same as for the corresponding reactions in the dyads.

The transient absorption spectra for the triad also contain a species with the signatures of the $*Ru^{II}$ excited state, and a lifetime of ca. 65 ns. This species is responsible for the long-lived emission around 625 nm, for the transient absorption at 370 nm in Figure 7b, and for a long-lived bleaching at 450 nm. This bleach counteracts the absorption from the $BQ^{\bullet-}$ resulting in a near zero difference absorption around 450 nm on the nanosecond time scale (Figure 7b). The magnitude of the signals from the long-lived $*Ru^{II}$ species increases with light exposure. The 65 ns lifetime is too short for being a simple, unsubstituted $[Ru(bpy)_3]^{2+}$ impurity, but it is similar to the lifetime of the PTZ−Ru^{II} dyad. We attribute this to a triad species in which the quinone is no longer functional. Because the charge-separated state is a diradical, it seems reasonable to assume that it can undergo coupling between $PTZ^{\bullet+}$ and $BQ^{\bullet-}$ to a PTZ−hydroquinone species which would have similar photophysical properties as the simple PTZ−Ru^{II} dyad, in accordance with experimental results. This assumption is supported by the fact that, in an irradiated sample, the NMR shows shifts toward higher field of some of the quinone protons around 6.5 ppm as well as changes in the signals of the PTZ-methylene protons at 5.3 ppm. The electrochemical data also suggest a possible reaction between a $PTZ^{\bullet+}$ radical and a neutral benzoquinone on different triad molecules. This new species was formed in light reactions but was present to a level of ca. 10% already in the first flash of a sample prepared in the dark. It is possible that some photodegradation of the triad occurred already during synthesis and workup, although care was taken to exclude light. On the basis of differential extinction coefficients, we estimate that the lower spectrum in Figure 7b is composed of ∼70% $PTZ^{\bullet+}-Ru^{II}-BQ^{\bullet-}$ and ∼30% of the $*Ru^{II}$ excited state of this light-generated impurity.

In both the PTZ containing complexes, we also observed a short-lived ($\tau < 20$ ns) emission around 530 nm in the nanosecond flash photolysis experiments, that grew in intensity with increasing number of laser flashes. This emission was also seen in the steady state emission spectra of the flashed samples. We have previously seen a similar behavior when we photooxidized the nitrogen of bispicene in a Ru^{II}−bispicene complex.[37] We therefore attribute the 530 nm emission to an oxidation product of PTZ. We do not know the mechanisms behind these decomposition reactions.

From the kinetics in Figure 2, the formation quantum yield of the charge-separated state $PTZ^{\bullet+}-Ru^{II}-BQ^{\bullet-}$ in the intact triads can be calculated to ≥90%, which is very high. This value is in agreement with the maximum transient absorption from $PTZ^{\bullet+}$ (Figure 7b) that corresponds to ca. 70% of the initial $*Ru^{II}$ concentration. With the estimated ca. 30% photodegradation in the spectra of Figure 7b, this suggests a charge separation yield of ca. 100% in the intact triad. We note that, in related PTZ−Ru^{II}−acceptor triads, the reported charge separation yields have in general not exceeded ca. 40%, so in that respect the present triad is performing much better. Although the kinetics of the charge separation steps was not always resolved in the previous studies, it seems the losses in yield were due to a slow secondary electron transfer, from PTZ to Ru^{III}, that did not compete as favorably with the $Ru^{III}-acceptor^{\bullet-}$ recombination as in our present triad. The anthraquinone-based triads of Meyer and co-workers[11,12] are on the other hand somewhat better in storing free energy ($\Delta G° = 1.54$ eV) in the charge-separated state, with a charge separation lifetime of 150−170 ns. The free energy ($\Delta G°$) stored in the $PTZ^{\bullet+}-Ru^{II}-BQ^{\bullet-}$ state is 1.32 eV, on the basis of the difference in $PTZ^{+/0}$ and $BQ^{0/-}$ redox potentials, that is 63% of the excitation energy (E_{00}) of 2.11

(37) Sun, L.; Berglund, H.; Davidov, R.; Norrby, T.; Hammarström, L.; Korall, P.; Börje, A.; Philouze, C.; Berg, K.; Thran, A.; Andersson, M.; Stenhagen, G.; Mårtensson, J.; Almgren, M.; Styring, S.; Åkermark, B. *J. Am. Chem. Soc.* **1997**, *119*, 6996−7004.

eV (assuming $\Delta S^\circ = 0$ for the excitation process). The lifetime of the charge-separated state is 80 ns, which is long enough even for rather slow secondary reactions to occur. It thus seems that the triad system has favorable properties for further use as an artificial charge separation center.

Conclusions

Three electron donor−acceptor dyads and triads have been synthesized and studied (Schemes 1 and 2), that display photoinduced electron transfer from the excited Ru^{II} moiety to the attached benzoquinone unit with a rate constant of $5 \times 10^9\ s^{-1}$ ($\tau = 200$ ps). Recombination to the ground state reactants followed, with a rate constant of ca. $4.5 \times 10^8\ s^{-1}$ ($\tau \sim 2.2$ ns) in both $Ru^{II}-BQ$ (**4**) and $Ru^{II}-BQ-Co^{III}$ (**6**), showing that a further electron−hole separation reaction $Ru^{III}-BQ^{\bullet -}-Co^{III} \rightarrow Ru^{III}-BQ-Co^{II}$ could not compete with the recombination reaction. To solve this problem, PTZ−Ru^{II}−BQ (**8**) was prepared, in which a fast electron donor, PTZ, was linked to the ruthenium in order to slow the recombination. This complex did form the fairly long-lived ($\tau = 80$ ns) charge-separated state $PTZ^{\bullet +}-Ru^{II}-BQ^{\bullet -}$ in high yield (>90%), that stored 1.32 eV of the excitation energy. It thus seems that the triad system is well suited for further use as an artificial charge separation center. Only one previous $[Ru(bpy)_3]^{2+}$-based triad has been reported to give a >40% charge separation yield,[16] and the common factor between that triad and ours seems to be a rapid secondary electron transfer from the PTZ to the photogenerated Ru^{III} moiety. Unfortunately, it turned out to be photolabile, at least partially due to an interesting coupling reaction between the $PTZ^{\bullet +}$ and $BQ^{\bullet -}$ moieties. Therefore, we were unable to prepare a PTZ−Ru^{II}−BQ−Co^{III} tetrad from PTZ−Ru^{II}−BQ. Finally, the dyad PTZ−Ru^{II} (**9**) was prepared as a model complex for the PTZ−Ru^{II} unit in PTZ−Ru^{II}−BQ. In the dyad, a reversible electron transfer was observed on excitation, with ΔG° close to zero. Thus, a quasiequilibrium was established with an observed time constant of 7 ns, with ca. 82% of the population in the PTZ−$*Ru^{II}$ state and 18% in the $PTZ^{\bullet +}-Ru^{II}(bpy^{\bullet -})$ state. These states decayed in parallel with an observed lifetime of 90 ns. The initial electron transfer to form the $PTZ^{\bullet +}-Ru^{II}(bpy^{\bullet -})$ state was thus faster than what would have been inferred from the $*Ru^{II}$ emission decay ($\tau = 90$ ns), a possibility that may have been overlooked in other similar systems with close to isoergonic electron transfer.

Experimental Section

Spectroscopy. The solvent used was acetonitrile of spectroscopic grade (Merck). UV−vis absorption spectra were measured on a Hewlett-Packard 8453 instrument or a Varian Cary 50 UV−vis spectrophotometer. The emission spectra were recorded on a SPEX-Fluorolog II fluorimeter. Spectra at 77 K were taken in dry butyronitrile solution in a coldfinger Dewar. The infrared spectra were recorded on a Perkin-Elmer Spectrum One spectrometer in KBr pellets. ^1H and ^{13}C NMR spectra were measured on Varian 300 or 400 MHz spectrometers or on a Bruker 500 MHz spectrometer. The MALDI-TOF experiments were performed on a Bruker BIFLEX III spectrometer equipped with pulsed ion extraction (PIE). 2,5-Dihydroxybenzoic acid (DHB) was used as matrix, and poly(ethylene glycol) (PEG) as internal standard. The ESI-MS experiments were carried out on a ZacSpec mass spectrometer (VG Analytical, Fisons Instrument), with nitrogen as bath and nebulizing gas.

The transient absorption pump−probe measurements were performed on a regenerative amplified Ti:sapphire system that has been described in detail previously.[38] The laser pulses generated had an average temporal width of 150 fs. Pump light was produced in an optical parametric amplifier (TOPAS) or by simple second harmonic generation in a BBO crystal. The intensity of the excitation light was set below 3 μJ to reduce the probability of two-photon excitation. The continuos probe light was generated in a sapphire or rotating CaF_2 crystal.

Time-resolved absorption and emission experiments on a nanosecond time scale were performed with a frequency tripled Q-switched Nd:YAG laser from Quantel producing <10 ns flashes. Pump light tunable in the range 410−660 nm was obtained in an OPO. The average energy of the laser pulses was ~15 mJ.

The samples were prepared with an absorption at 452 nm ($\epsilon = 1.3 \times 10^4\ M^{-1}\ cm^{-1}$)[2] of ca. 0.3 for transient absorption experiments and ca. 0.1 for emission experiments. In the emission and flash photolysis experiments, the samples were purged with nitrogen. All the kinetic results presented are averages of ca. 10 independent measurements.

Electrochemistry. Cyclic voltammetry and differential pulse voltammetry were carried out with a three-electrode setup in a three-compartment cell connected to an Autolab potentiostat with a GPES electrochemical interface (Eco Chemie). The working electrode was a glassy carbon disk. Potentials were measured versus a nonaqueous Ag/Ag^+ reference electrode (CH Instruments, 10 mM $AgNO_3$ in CH_3CN). All potentials reported here are referenced versus the Fc^+/Fc couple by adding −0.080 V to the potentials measured versus the Ag/Ag^+ electrode. IR drop was not compensated for, resulting in peak to peak separations of $\Delta E_p = 88$ mV ($\upsilon = 0.1\ V\ s^{-1}$) and $\Delta E_p = 78$ mV ($\upsilon = 0.05\ V\ s^{-1}$) for the reversible Fc^+/Fc couple. Solutions were prepared from dry CH_3CN (Merck, spectroscopy grade, dried with MS 3 Å) and contained ca. 1 mM of the analyte and 0.1 M tetrabutylammonium hexafluorophosphate (Fluka, electrochemical grade, dried at 373 K) as supporting electrolyte. The glassware used was oven dried, assembled, and flushed with argon while hot. All measurements were performed under argon atmosphere.

Materials. All reagents were purchased commercially and used without further purification. The concentration of *n*-BuLi was determined by titration with diphenylacetic acid. Diisopropylamine was distilled from NaH and stored over KOH. THF was freshly distilled from Na/benzophenone before use. DMF was distilled from CaH_2 and stored over molecular sieves (4 Å). Other solvents were used as received. All reactions and purifications involving donor/acceptor metal complexes were performed under reduced light. Chromatographic purifications were carried out on silica gel 60 (230−400 mesh), and thin-layer chromatography was performed on Merck silica gel 60 F_{254} or aluminum oxide 60 F_{254} neutral.

Synthesis. 2,6-Dibromomethyl-1,4-dimethoxybenzene (**1**),[23] 4-bromomethyl-4′-methyl-2,2′-bipyridine,[25] 10-((4′-methyl-2,2′-bipyridin-4-yl)methyl)phenothiazine (PTZdmb),[14] *cis*-$Ru(bpy)_2Cl_2 \cdot 2H_2O$,[39] *cis*-$Ru(DMSO)_4Cl_2$,[24] $Ru(bpy)(DMSO)_2Cl_2$,[40] $[Co(bpy)_2$-

(38) Andersson, M.; Davidsson, J.; Hammarström, L.; Korpi-Tommola, J.; Peltola, T. *J. Phys. Chem. B* **1999**, *103*, 3258−3262.
(39) Lay, P. A.; Sargeson, A. M.; Taube, H. *Inorg. Synth.* **1986**, *24*, 291−299.

Cl_2]Cl·5H_2O,[41] and [Co(bpy)$_3$]Cl_3[42] were prepared as described elsewhere. *N*-Methyl phenothiazine (MePTZ) was prepared by methylation of phenothiazine by CH_3I in THF.[43] [Co(bpy)$_3$](PF_6)$_3$ was isolated by dissolving the chloride salt in MeOH and precipitating with an excess of NH_4PF_6.

2,6-Bis(2-(4-methyl-2,2′-bipyrid-4′-yl)-etyl)-1,4-dimethoxybenzene (2). Diisopropylamine (0.95 mL, 6.8 mmol) was added to freshly distilled THF (15 mL) under nitrogen. To this solution was slowly added *n*-BuLi (4.5 mL, 7.2 mmol). The solution was left at room temperature for 45 min before it was reduced to −78 °C, and dmb, 4,4′-dimethyl-2,2′-bipyridine, (1.20 g, 6.51 mmol) in THF (35 mL) was added dropwise. After 2 h, the dark-brown solution was warmed to room temperature and added dropwise to a solution of **1** (0.80 g, 2.47 mmol) in THF (35 mL) at −78 °C. The solution was left overnight. H_2O was added and the ether phase separated. The H_2O phase was extracted with additional Et_2O. The combined organic phases were dried over Na_2SO_4 and the solvent removed to give a yellow/brown oil. This was chromatographed on silica (eluent: gradient 3−3.5% EtOH/CH_2Cl_2, 1% NH_3) to give **2** as a slightly yellow oil which crystallized on standing (1.00 g, 78%). ^{1}H NMR (300 MHz, $CDCl_3$, 25 °C): δ 8.54 (d, 2H), 8.52 (d, 2H), 8.28 (s, 2H), 8.21 (s, 2H), 7.14−7.08 (m, 4H), 6.57 (s, 2H), 3.70 (s, 3H), 3.68 (s, 3H), 2.97 (s, 8H), 2.40 (s, 6H). ^{13}C NMR (300 MHz, $CDCl_3$, 25 °C): δ 156.4, 156.1, 155.8, 152.0, 150.5, 149.2, 149.1, 148.3, 135.2, 124.9, 124.1, 122.2, 121.4, 113.6, 61.9, 55.8, 36.7, 31.7, 21.6.

Complex 3. *cis*-Ru(bpy)$_2$$Cl_2$·2$H_2O$ (0.057 g, 0.11 mmol) and **2** (0.350 g, 0.66 mmol, 6 equiv) were added to degassed EtOH (25 mL), and the solution was heated under nitrogen at reflux. After 4 h, the red solution was cooled to room temperature, and the volume was reduced in vacuo to 5 mL. H_2O (10 mL) was added, and the solution was washed with CH_2Cl_2. An excess of NH_4PF_6 was added, and the resulting solid was redissolved by addition of CH_2Cl_2. The organic phase was separated and the H_2O phase extracted with additional CH_2Cl_2. The combined organic phases were evaporated in vacuo, and the resulting solid was redissolved in acetone and precipitated by dropwise addition of Et_2O to give **3** (0.090 g, 67%). ^{1}H NMR (500 MHz Bruker, CD_3CN, 25 °C): δ 8.48 (d, 1H), 8.43 (d, 1H), 8.38 (d, 1H), 8.28−8.23 (m, 4H), 8.17 (s, 1H), 8.03 (t, 1H), 8.00−7.90 (m, 3H), 7.81 (t, 1H), 7.73 (d, 1H), 7.71 (d, 1H), 7.67 (d, 1H), 7.65−7.60 (m, 3H), 7.57 (d, 1H), 7.42−7.35 (m, 2H), 7.34−7.25 (m, 3H), 7.18 (d, 1H), 7.14 (d, 1H), 7.10 (d, 1H), 6.71 (d, 1H), 6.60 (d, 1H), 3.68 (s, 3H), 3.57 (s, 3H), 3.14 (m, 1H), 3.08−2.98 (m, 3H), 2.82−2.68 (m, 3H), 2.55 (m, 1H), 2.52 (s, 3H), 2.47 (s, 3H). ESI-MS: *m*/*z* [M − PF_6^-]$^+$ 1089.091 (calcd for $C_{54}H_{50}N_8O_2RuPF_6$: 1089.276), [M − 2PF_6^-]$^{2+}$ 471.774 (calcd for $C_{54}H_{50}N_8O_2Ru$: 472.156).

Complex 4. Complex **3** (0.190 g, 0.15 mmol) was dissolved in CH_3CN (10 mL), and CAN, cerium ammonium nitrate, (0.240 g, 0.44 mmol) in H_2O (10 mL) was added dropwise. The solution was left stirring at room temperature for 1.5 h after which H_2O (15 mL) was added. The solution was extracted with CH_2Cl_2 and the organic phase washed with H_2O. The solvent was removed to give **4** (0.134 g, 72%). The solid was chromatographed once on silica (eluent: CH_3CN/H_2O/sat. KNO_3, 20:3:1) before continuing, and an additional time (same eluent) before photolysis measurements to remove possible minute impurities. ^{1}H NMR (400 MHz, CD_3CN, 25 °C): δ 8.59 (d, 1H), 8.50 (d, 1H), 8.48−8.41 (m, 4H), 8.38 (s, 1H), 8.34 (s, 1H), 8.31 (s, 1H), 8.15 (s, 1H), 8.06−7.96 (m, 4H), 7.74−7.66 (m, 4H), 7.59 (d, 1H), 7.54 (d, 1H), 7.46 (d, 1H), 7.45−7.33 (m, 5H), 7.26−7.21 (m, 2H), 6.51 (s, 2H), 3.04−2.98 (m, 2H), 2.95−2.89 (m, 2H), 2.84−2.79 (m, 2H), 2.77−2.71 (m, 2H), 2.54 (s, 3H), 2.53 (s, 3H). IR (KBr): 1653 cm^{-1} (C═O). ESI-MS: *m*/*z* [M − PF_6^-]$^+$ 1059.017 (calcd for $C_{52}H_{44}N_8O_2RuPF_6$: 1059.229), [M − 2PF_6^-]$^{2+}$ 456.736 (calcd for $C_{52}H_{44}N_8O_2Ru$: 457.132). Anal. Calcd (%) for $C_{52}H_{44}N_8O_2RuP_2F_{12}$·1.25$CH_2Cl_2$ (1310.15): C 48.82, H 3.58, N 8.55. Found: C 48.77, H 3.57, N 8.44.

2,6-Bis(2-(4-methyl-2,2′-bipyrid-4′-yl)-etyl)-1,4-benzoquinone (5). Compound **2** (1.10 g, 2.07 mmol) and *p*-toluenesulfonic acid monohydrate (0.79 g, 4.13 mmol) were dissolved in CH_3CN (30 mL). CAN (3.40 g, 6.21 mmol) dissolved in H_2O (25 mL) was added in portions. The stirred solution was left at room temperature for 45 min. Saturated Na_2CO_3 was added until pH = 7, CH_2Cl_2 was added to the suspension, and the mixture was filtered. The CH_2Cl_2 phase was separated and washed with H_2O. The organic phase was dried over Na_2SO_4 and evaporated in vacuo. The remaining solid was chromatographed on a short silica column (eluent: CH_2Cl_2, 3% EtOH) to give **5** as a yellow solid (0.70 g, 68%). ^{1}H NMR (300 MHz, $CDCl_3$, 25 °C): δ 8.57 (d, 2H), 8.52 (d, 2H), 8.25 (m, 2H), 8.22 (m, 2H), 7.13 (d, 2H), 7.12 (d, 2H), 6.49 (s, 2H), 2.94−2.78 (m, 8H), 2.42 (s, 6H). ^{13}C (300 MHz, $CDCl_3$, 25 °C): δ 187.5, 187.3, 156.7, 155.9, 150.5, 149.5, 149.2, 148.4, 148.1, 133.2, 125.0, 123.9, 122.3, 121.3, 33.8, 30.3, 21.4. IR (KBr): 1652 cm^{-1} (C═O).

Dinuclear Complex 6. Complex **4** (0.038 g, 3.2·10^{-5} mol) and [Co(bpy)$_2$$Cl_2$]Cl·5$H_2O$ (0.022 g, 4.2 × 10^{-5} mol) were added to degassed MeOH (20 mL). The mixture was heated to reflux under nitrogen for 75 min. The solvent was removed and the solid redissolved in H_2O. A saturated solution of NH_4PF_6 was added, and the formed precipitate was collected by filtration and washed repeatedly with H_2O and Et_2O to give **6** (0.046 g, 72%). ^{1}H NMR (400 MHz, CD_3CN, 25 °C): δ 8.70−8.64 (m, 4H), 8.56 (s, 1H), 8.55 (s, 1H), 8.50−8.44 (m, 8H), 8.38 (s, 1H), 8.37 (s, 1H), 8.08−8.00 (m, 4H), 7.78−7.68 (m, 8H), 7.60−7.50 (m, 4H), 7.46−7.36 (m, 4H), 7.30−7.20 (m, 6H), 7.16−7.04 (m, 2H), 6.52 (s, 1H), 6.49 (s, 1H), 3.15−3.08 (m, 2H), 3.04−2.96 (m, 2H), 2.88−2.76 (m, 4H), 2.65 (s, 3H), 2.53 (s, 3H). IR (KBr): 1653 cm^{-1} (C═O). ESI-MS: *m*/*z* [M − 2PF_6^-]$^{2+}$ 860.090 (calcd for $C_{72}H_{60}N_{12}O_2CoRuP_3F_{18}$: 860.113), [M − 3$PF_6^-$]$^{3+}$ 525.106 (calcd for $C_{72}H_{60}N_{12}O_2CoRuP_2F_{12}$: 525.088), [M − 4$PF_6^-$]$^{4+}$ 357.578 (calcd for $C_{72}H_{60}N_{12}O_2CoRuPF_6$: 357.574). Anal. Calcd (%) for $C_{72}H_{60}N_{12}O_2CoRuP_5F_{30}$ (2010.184): C 43.02, H 3.01, N 8.36. Found: 42.91, H 3.16, N 8.27.

Complex 7. Ru(bpy)(DMSO)$_2$$Cl_2$ (0.290 g, 0.60 mmol) and PTZdmb (0.228 g, 0.60 mmol) were added to freshly distilled DMF (60 mL). The solution was heated at reflux under nitrogen for 2.5 h. The solvent was removed in vacuo, H_2O (10 mL) was added to the remaining solid, and the mixture was stirred for 30 min. Filtration of the mixture gave a black solid which was repeatedly washed with H_2O and Et_2O until colorless washings. The solid obtained was not further purified (0.351 g). MALDI-TOF: *m*/*z* [M − 2Cl^- + DHB^-]$^+$ 792.09 (calcd for $C_{41}H_{32}N_5O_4S_1Ru$: 792.12).

Complex 8. Ru(bpy)(PTZdmb)Cl_2 (**7**) (0.083 g, ca. 0.12 mmol) and **5** (0.293 g, 0.59 mmol) were added to degassed EtOH (30 mL), and the mixture was heated at reflux under nitrogen for 4 h. The solvent was removed, H_2O (10 mL) and CH_2Cl_2 (10 mL) were added, the H_2O phase separated and washed with additional CH_2Cl_2. The combined organic phase was extracted once with H_2O.

(40) Zakeeruddin, S. M.; Nazeeruddin, Md. K.; Humphry-Baker, R.; Grätzel, M. *Inorg. Chem.* **1998**, *37*, 5251−5259.
(41) Hancock, M. P.; Josephsen, J.; Schäffer, C. E. *Acta Chem. Scand.* **1976**, *30*, 79−97.
(42) Crumbliss, A. L.; Perine, S. C.; Edwards, A. K.; Rillema, D. P. *J. Phys. Chem.* **1992**, *96*, 1388−1394.
(43) Bae, J. Y.; Ranjit, K. T.; Luan, Z.; Krishna, R. M.; Kevan, L. *J. Phys. Chem. B* **2000**, *104*, 9661−9669.

To the combined H_2O phases were added an excess of NH_4PF_6 and CH_2Cl_2. The organic phase was separated and the solvent removed. The crude product was chromatographed on silica (eluent: CH_3CN/H_2O/sat. KNO_3 20:3:1). The red-brown solid was chromatographed two additional times and isolated as PF_6^- salt (0.017 g, ca. 10%). ^1H NMR (400 MHz, CD_3CN, 25 °C): δ 8.50−6.70 (34H, aromatic), 6.56−6.40 (2H, Q), 5.32−5.23 (4 singlets, CH_2PTZ), 3.05−2.60 (8H, CH_2-groups), 2.55−2.40 (9H, CH_3-groups). IR (KBr): 1652 cm^{-1} (C═O). ESI-MS: *m*/*z* $[M - PF_6^-]^+$ 1284.434 (calcd for $C_{66}H_{55}N_9O_2SRuPF_6$: 1284.290), $[M - 2PF_6^-]^{2+}$ 569.693 (calcd for $C_{66}H_{55}N_9O_2SRu$: 569.663).

Complex 9. This complex was prepared in two steps without characterization of the intermediate product, $Ru(bpy)(dmb)Cl_2$. $Ru(bpy)(DMSO)_2Cl_2$ (0.100 g, 0.21 mmol) and dmb (0.038 g, 0.21 mmol) were added to freshly distilled DMF (30 mL), and the mixture was heated at 120 °C under nitrogen for 3 h. The solvent was evaporated in vacuo, and PTZdmb (0.081 g, 0.21 mmol) and EtOH (25 mL) were added. The mixture was degassed, and the solution was heated at reflux under nitrogen for 7 h. The solvent was removed, and H_2O (15 mL) was added and the clear red solution washed with CH_2Cl_2. Additional CH_2Cl_2 and an excess of NH_4PF_6 were added, and the CH_2Cl_2 phase was separated and the H_2O phase extracted once more with CH_2Cl_2. The combined organic phases were washed with H_2O and evaporated to dryness, and the residue was chromatographed twice on silica (eluent: CH_3CN/H_2O/sat. KNO_3, 40:4:1) and isolated as PF_6^- salt (0.049 g, 21%). ^1H NMR (400 MHz, CD_3CN, 25 °C): δ 8.60−6.70 (28H, aromatic), 5.32−5.31 (2 singlets, CH_2PTZ), 2.55−2.50 (9H, CH_3-groups). ESI-MS: *m*/*z* $[M - PF_6^-]^+$ 968.225 (calcd for $C_{46}H_{39}N_7SRuPF_6$: 968.168), $[M - 2PF_6^-]^{2+}$ 411.641 (calcd for $C_{46}H_{39}N_7SRu$: 411.602). Anal. Calcd (%) for $C_{46}H_{39}N_7SRuP_2F_{12}$ (1112.913): C 49.64, H 3.53, N 8.81. Found: C 49.81, H 3.67, N 8.61.

Acknowledgment. This work was financially supported by grants from the Knut and Alice Wallenberg Foundation, the Swedish National Energy Administration, and the Swedish Science Research Council (VR). We thank Jerker Mårtensson at Chalmers University of Technology, Göteborg, Sweden, for the mass spectrometry measurements. We also thank Stenbjörn Styring at the Department of Biochemistry, University of Lund, Sweden, for stimulating discussions.

Supporting Information Available: Detailed description of kinetics calculations and NMR figures. This material is available free of charge via the Internet at http://pubs.acs.org.

IC020606J